RSC Advances

PAPER

View Article Online
View Journal | View Issue

Cite this: *RSC Adv.*, 2024, **14**, 12665

Innovative surfactant-free synthesis of core–shell SiO_2/ZnO particles: rapid ultrasonication and photocatalytic inhibition†

Lailatul Qomariyah, *[a] Tomoyuki Hirano, [b] Nicky Rahmana Putra, [c] Suprapto Suprapto,[a] Hendrix Abdul Ajiz [d] and Mar'atul Fauziyah [e]

This study demonstrates the preparation of SiO_2/ZnO core–shell nanoparticles with controllable shell size and their optical properties. A facile ultrasonication method was utilized to prepare the core–shell particles in the absence of surfactant materials. The synthesis duration was 75% shorter than that required for the common sol–gel method, which favours its potential applicability in the future for mass production. Tetraethyl orthosilicate (TEOS) was used as the silica source, while the core material was prepared using zinc acetate dihydrate. The outer shell size could easily be controlled by changing the molar ratio of silica from 0.25 to 1.00. The experimental results show that increasing the silica ratio was effective in suppressing the self-agglomeration of ZnO and, further, in obtaining agglomeration-free particles. The investigation of the photoluminescence (PL) properties of nanometre-sized ZnO revealed several emission peaks in the ultraviolet (UV) wavelength range, indicating variations in bandgap energy. This did not appear in the spectrum of micrometre-sized ZnO particles. The core–shell particles produced with higher amounts of silica showed higher UV-A and UV-B absorption. In addition, the presence of silica reduced the photocatalytic activity of ZnO by 65% and reduced the PL intensity. The obtained emission peaks, intensity changes, and spectral characteristics open new avenues for further research on tailoring the properties of SiO_2/ZnO core–shell structures for specific technological advancements. These advancements hold promising applications in UV attenuation materials, LED technologies, lenses, and solar cells within the realm of optical devices.

Received 20th February 2024
Accepted 5th April 2024

DOI: 10.1039/d4ra01309c

rsc.li/rsc-advances

Introduction

In recent decades, there has been a growing interest in UV attenuation materials and photoluminescent substances because of the increasing demand for effective UV shielding materials.[1–4] Zinc-based materials exhibit significant potential in UV shielding, primarily, owing to their wide bandgap of approximately 3.36 eV.[5,6] The inherent properties of ZnO particles further enhance their suitability for application in UV attenuation.[7–9] However, ZnO has high photocatalytic activity and a wide bandgap energy.[10–13] This hinders UV-shielding applications due to the occurrence of oxidation–reduction reactions. In general, ZnO particles show excellent UV-shielding properties in the UV-A and UV-B region.[14,15] Therefore, they are mostly employed in sunscreens.[16–19] However, their higher surface energy leads to their easy agglomeration. To overcome this limitation, an inert material, such as silica particles, is added during the synthesis process.[20,21]

Nanoscale ZnO particles have a large surface energy and surface area.[22–26] This results in difficulties in introducing silica particles on the ZnO surface as a coating material. Previous studies have reported that the addition of a surfactant can potentially facilitate the introduction of silica particles as a shell material to further improve particle properties. Mishra *et al.*[27] reported that functionalized silica-coated zinc oxide nanoparticles with the addition of CTAB as the surfactant exhibited an increased PL intensity. Similar results were also reported by Ajiz *et al.*[28] when an anionic surfactant was added during the formation of ZnO/SiO_2 *via* a spray-drying method using various zinc ratios. This resulted in a significant increase in PL intensity with increasing zinc amounts.

[a]*Department of Industrial Chemical Engineering, Institut Teknologi Sepuluh Nopember, Surabaya, 60111, Indonesia. E-mail: laila.qomariyah@its.ac.id*

[b]*Chemical Engineering Program, Graduate School of Advanced Science and Engineering, Hiroshima University, 1-4-1 Kagamiyama, Higashihiroshima, Hiroshima 739-8527, Japan*

[c]*Research Center for Pharmaceutical Ingredients and Traditional Medicine, National Research and Innovation Agency (BRIN), Complex Cibinong Science Center-BRIN, Cibinong 16911, Jawa Barat, Indonesia*

[d]*Department of Chemical Engineering, Institut Teknologi Sepuluh Nopember, Surabaya, 60111, Indonesia*

[e]*Department of Chemical Engineering, Faculty of Engineering, Universitas Brawijaya, Malang, 65145, Indonesia*

† Electronic supplementary information (ESI) available. See DOI: https://doi.org/10.1039/d4ra01309c

Widiyastuti *et al.*[29] prepared SiO_2/ZnO nanoparticles using a flame spray-drying method without the addition of any surfactant, demonstrating a good UV-blocking material with high PL intensity. However, the produced particles had a non-core–shell morphology and showed agglomeration. Several shortcomings related to controlling the particle morphology and successful silica introduction on the ZnO surface persist. In addition, problems exist in achieving core–shell particles of homogeneous size in the nanometre scale. In this study, the preparation of SiO_2/ZnO core–shell particles using a fast ultrasonication method was successfully accomplished in the absence of surfactants. The optical properties and PL performance of the prepared core–shell particles were also tested. As the presence of different amounts of silica particles can affect the produced core–shell properties, the effects of silica ratio on the particle characteristics were investigated.

Introducing silica particles onto the surface of the ZnO particles without surfactants using the Stöber method is a challenging yet viable approach.[30–32] There are two potential strategies to achieve this: adding the silica particles during the growth of the ZnO particles or after the growth process. The latter method entails synthesizing ZnO separately, followed by the addition of silica particles as a coating material. However, the latter method is time-consuming and involves multiple processes. The first strategy is considered effective because it allows the simultaneous nucleation of silica particles along with the growth of ZnO, resulting in the formation of core–shell particles.

In general, many synthesis methods of SiO_2/ZnO core–shell particles have been elaborated; the recent one being the spray pyrolysis method.[33–35] However, this method has several shortcomings related to the expensive apparatus and high energy consumption due to high-temperature conditions. Other synthesis methods, such as hydrothermal and solvothermal methods, produce good-quality products but also consume higher energy and involve processes requiring high pressure.[36–38] In addition, it produces inhomogeneous and agglomerated nanoparticles. The sol–gel method is effective in producing homogeneous nanoparticles at low-temperature conditions.[39]

However, it has limitations due to the multistep process. To overcome these limitations, the utilization of ultrasonication methods is an effective way to produce nanoparticles in minutes with low energy consumption. They can produce agglomeration-free core–shell particles with high dispersibility and uniform particle size. The ultrasonication method is a rapid process, and the reaction occurs at the nanometre scale,[40–42] allowing the formation of the core–shell nanostructure. In addition, these nanoparticles might potentially possess PL properties, which can be applied in very small devices.

In summary, this work aims to produce core–shell SiO_2/ZnO particles *via* an ultrasonication method for application as a UV-shielding material. Short production time could be achieved by this method. The effect of the amount of silica particles on the ZnO surface on the optical properties was investigated thoroughly by varying the concentration of TEOS added during the synthesis process. Different from the previously reported ultrasonication methods, the production of the SiO_2/ZnO core–shell particle was achieved in the absence of surfactant materials. The ultrasonic energy could promote the nucleation of TEOS on the ZnO surface, where the reaction takes place at the nanoscale. The experimental results show that under appropriate synthesis conditions, ultrasonication can be employed as an effective method to obtain core–shell particles with controllable properties. The presence of silica particles was found to affect the particle properties, especially the optical properties required for its application as a UV-shielding material.

Experimental details

Materials and methods

Materials. All the chemicals used in this experiment were of analytical grade and directly used without further purification. Zinc acetate dihydrate [$Zn(CH_3COO)_2 \cdot 2H_2O$, 99.5%] of reagent grade was purchased from Merck and used as the ZnO source. Tetraethyl orthosilicate (TEOS, 99.9%) the silica source, was purchased from Merck Chemical Company, Germany. Sodium hydroxide (NaOH, 99.9%), methyl alcohol (MeOH, 99.5%) and ultrapure water of reagent grade p.a. were obtained from Sigma-Aldrich Company, Ltd, USA.

Methods

Preparation of the SiO_2/ZnO core–shell structures. The schematic of the core–shell synthesis is given in Fig. 1. Zinc acetate was added to methanol as the ZnO source to obtain a 0.1 M solution concentration. Then, the solution was homogenized using an ultrasonication probe for 10 minutes to obtain a dispersed solution. TEOS and 0.1 M NaOH solution were then added to the zinc acetate solution. The resulting mixture was stirred continuously using the ultrasonication probe for 30 minutes until the reaction was complete. The white precipitate that appeared at the bottom of the flask was then separated from the solution by centrifugation at 4000 rpm for 20 min. The precipitate was washed three times with ultrapure water and ethanol followed by oven drying at 120 °C. To control the thickness, the SiO_2/ZnO molar ratio was varied from 0.25 to 1.00.

The morphology was examined using transmission electron microscopy (TEM; JEM-2010, 200 kV, JEOL Ltd, Tokyo, Japan). The particle size and shell thickness were measured from the TEM images of 200 randomly selected particles. The Fourier transform infrared (FT-IR; Agilent) spectra of the core–shell particles were recorded to investigate the chemical bonding in the particles. The crystallinity of the produced core–shell particles was measured using X-ray diffractometry (XRD) at angles in the range of $2\theta = 10$–$80°$. Their optical transmission was measured using ultraviolet-visible (UV-vis) spectroscopy (Cary 60, Agilent, United States). The excitation and emission luminescence spectra of the core–shell particles were measured using a luminescence spectrometer (Shimadzu RF-6000, Japan) equipped with a xenon source.

Photocatalytic activity test. Typically, 2 mg of core–shell particles were dispersed in 100 mL of 10 ppm methylene blue (MB) solution. The mixture was then stirred in the dark for 30

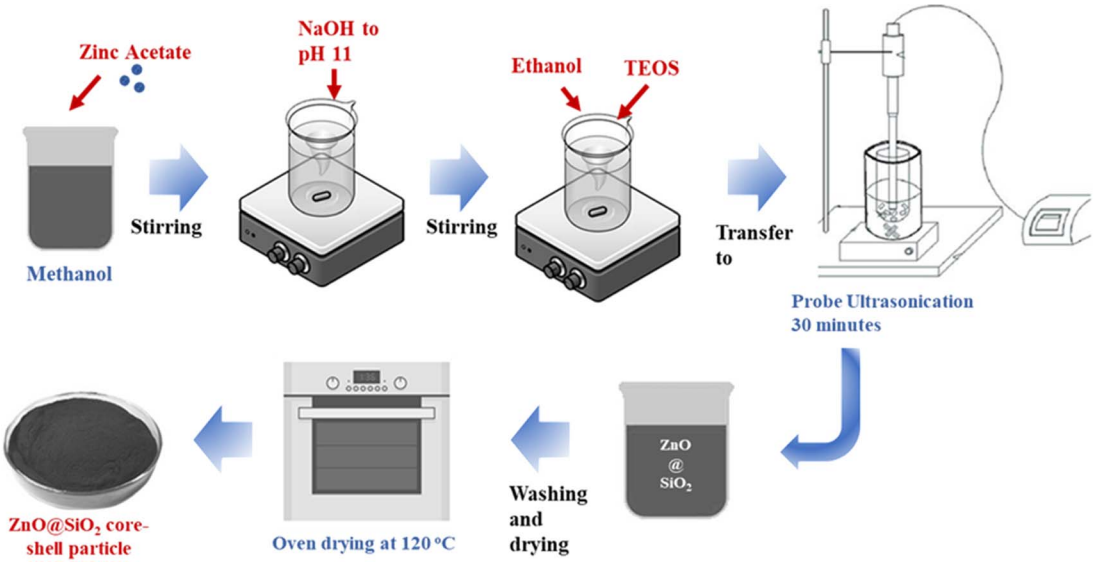

Fig. 1 Schematic of the preparation of core–shell SiO_2/ZnO particles.

minutes to investigate the adsorption–desorption mechanism. The time-dependent photocatalytic test was conducted as follows. After 30 minutes in the dark conditions, 10 mL was taken from the solution for absorbance measurements using UV-vis spectroscopy. Then, the remaining solution was subjected to direct sunlight irradiation for 180 minutes. A luxmeter was used to measure the sunlight intensity during the photocatalytic reactions, and the values ranged from 70 000 to 100 000 lux. To obtain this kind of sunlight intensity, the experiment was conducted from 11.00 a.m. to 2.00 p.m. in the summer season in Surabaya, Indonesia. During the photocatalytic test, 10 mL of the sample solutions were drawn every 30 minutes. Then, the absorbance of the samples was measured using UV-vis spectroscopy. The degradation of the MB solution was calculated using the following equation:

$$\text{Degradation rate } (\%) = \frac{C_0 - C}{C_0} \times 100\% = \frac{A_0 - A}{A_0} \times 100\% \quad (1)$$

where C_0 is the initial concentration of the pollutant, C is the concentration after the photocatalytic reaction for a definite time (t), A_0 is the initial absorbance of the pollutant, and A is the absorbance after t min of photocatalytic reaction. A similar procedure was followed to check the photocatalytic activity of the core–shell particles in the methyl orange (MO) solution.

Results and discussion

The formation of the core–shell particles during the synthesis process was initiated by the formation of ZnO from zinc acetate *via* the principle described in our previous work.[43] The nucleation of TEOS occurred on the ZnO surface, as illustrated in Fig. 2. The main event that controls shell formation is heterogeneous diffusion nucleation with ZnO as the "foreign body".[44,45] The nucleation of TEOS was accelerated by the ultrasonication process, in which fast mixing promotes cavitation in the solution. This cavitation enables a large contact area between TEOS and water. The presence of methanol also promotes a fast hydrolysis reaction to yield silicic acid ($Si(OH)_4$), the monomer of silica particles. The growth of the silica shell started immediately after the addition of TEOS and the sodium hydroxide solution to the solution of zinc acetate and methanol, as shown in Fig. 2(a). Qomariyah *et al.*[43] proposed that the nucleation mechanism of silica particles in a foreign body involves hexagonal zinc oxide particles as the template. After the nucleation of SiO_2 on the ZnO surface, TEOS undergoes a hydrolysis and condensation process under basic conditions to form the silica shell. Each reaction is enhanced by the ultrasonication treatment. The cavitation phenomenon that occurs during ultrasonication involves the growth and collapse of microbubbles, which promote the TEOS hydrolysis reaction. Further investigation of the TEM images showed that the ZnO particles possessed multiple cores, as seen in Fig. 2(a). This can be attributed to the agglomerated initial state of the ZnO particles. However, the ultrasonic treatment decreases the agglomerated state of the ZnO particles. In addition, the silica particles also can be used to suppress ZnO agglomeration by trapping them in the silica matrix. Therefore, the agglomeration of the produced particles is hindered. The successful synthesis of the core–shell particles is shown by the TEM image in Fig. 2(a). The transparent outer particles are the silica particles, which perfectly cover the ZnO particles.

The formation of silica particles on the ZnO surface was confirmed by the XRD results, as shown in Fig. 2(b). Pure ZnO particles, which served as the template, possessed a hexagonal wurtzite crystal and perfectly matched with JCPDS no. 36-1641. The ZnO spectral peaks were retained in the core–shell particle spectrum but with a lower intensity. This implies the perfect coverage of the ZnO particles by amorphous SiO_2. Notably, the wurtzite structure was retained, according to the XRD pattern,

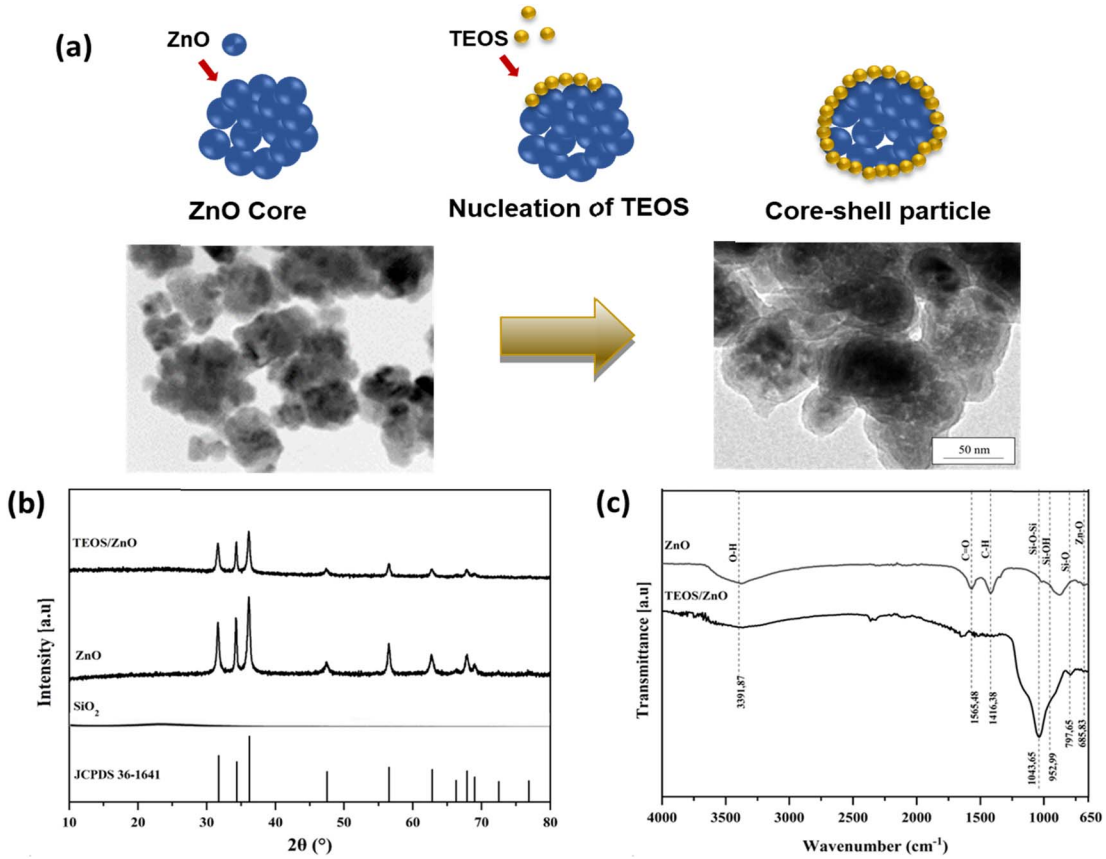

Fig. 2 (a) Schematic of the nucleation of TEOS on the ZnO particle, (b) XRD patterns of the SiO_2/ZnO, ZnO and SiO_2 particles, (c) FTIR spectra of the ZnO and SiO_2/ZnO particles.

indicating that the silica shell did not change the crystalline structure of the ZnO particles. The FT-IR spectra depicted in Fig. 2(c) confirm the chemical bonding of the ZnO template and the presence of SiO_2 in the core–shell particles. The reduction peaks at 685 and 1565 cm^{-1} could be assigned to the vibration of the Zn–O bond, which is characteristic of the ZnO particles that act as the core. The presence of SiO_2 particles on the core–shell particles was indicated by the sharp peak at around 1043 cm^{-1} assigned to the asymmetric vibration of the Si–O–Si bridging bonds, which convinced the formation of siloxane links on the surface of the ZnO template. A band was also observed near 797 cm^{-1} and could be assigned to the Si–O bridging bond. The broad peaks at around 3391 cm^{-1} correspond to the hydroxyl group O–H stretching vibration. The characteristic peaks of the ZnO particles were retained in the FT-IR spectrum of the core–shell particles. Both XRD and FT-IR spectra confirm the successful formation of the core–shell structure.

The effect of silica loading on the formation of the core–shell morphology was investigated. Fig. 3 shows the TEM images of the core–shell particles prepared under different SiO_2/ZnO ratios: 0.25, 0.5, 0.75, and 1.00. All particles present a core–shell structure, and no dense silica particles are observed. This implies that the heterogeneous nucleation of TEOS occurred completely on the ZnO surface, and the amount of TEOS was sufficient to cover the ZnO surface. The core–shell particles prepared at a ratio of 0.25 resulted in an agglomerated state even with ultrasonication. This is because the ZnO particles exist in an aggregate state. However, increasing the amount of silica particles to a molar ratio of 1.00 produced better-dispersed particles. The presence of silica particles can potentially minimize the interaction between many neighbouring ZnO particles at once during core–shell formation. The distance between the ZnO particles would then decrease, further suppressing ZnO and thereby yielding more dispersed core–shell particles. The TEM image in Fig. 3 also confirms that the variation in TEOS amount produces different core–shell characteristics. The particle size and shell thickness increased as the ratio of TEOS was increased. A thicker cell could be produced by adding high TEOS concentrations, and therefore, more silica particles were attached to the surface of the ZnO particles.

The shell thickness marked in the TEM images was measured through experimental and theoretical approaches. The theoretical shell thickness was determined by calculating the amount of ZnO and SiO_2 involved in the synthesis process, while the actual value was measured from the TEM image. In the theoretical approach, because heterogeneous nucleation takes place during the synthesis process, the number of ZnO particles N_Z can be approximated from the number of zinc acetate molecules involved in the reaction, denoted as N_{Za}. The

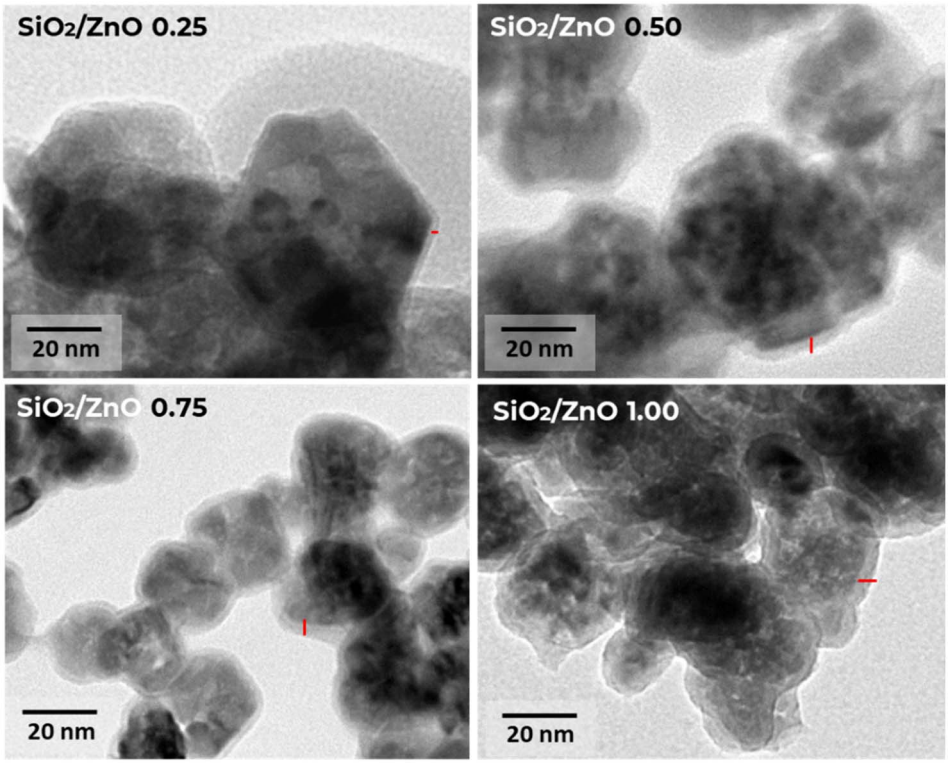

Fig. 3 TEM images of the SiO_2/ZnO core–shell particles prepared under different molar SiO_2/ZnO ratios.

number of SiO_2 particles in the shell can determined from the amount of TEOS added to the solution. In the typical condition of heterogeneous nucleation, the growth of nuclei on the foreign body, in this case ZnO, depends on the distance between the ZnO particles, which is generally equal. Therefore, the number of produced core–shell particles is equal to the number of ZnO particles, as shown in eqn (2). However, in actual conditions, the ZnO particles are randomly distributed, and this affects the distance between the neighbouring ZnO particles. As a result, inhomogeneous nucleation occurs on the ZnO surface, and not all ZnO particles are covered by silica particles. The aggregation of the ZnO particles also affects the number of silica shells. Even in the aggregated condition, ZnO has a narrow particle size, causing the produced core–shell particles to also have a narrow particle size distribution. The a^* factor is added to the equation as the correction factor that represents the number of ZnO particles fully covered by SiO_2. Eqn (3) can be re-written as follows:

$$N_Z = N_{Za} \tag{2}$$

$$N_Z \approx a^* N_{Za} \approx \left(\frac{a^* m}{\frac{3}{4}\pi\rho r^3} \right)_{Za} \tag{3}$$

where m (kg), ρ (kg m^{-3}), and r (m) denote the mass, density, and radius of zinc acetate particles, which convert to zinc oxide, respectively. The amount of silica particles in the shell (m_{shell}) could be determined from the mass balance equation. The mass of silica would be equal to the amount of TEOS converted to silica particles on the ZnO surface, which is expressed in eqn (4).

$$m_{shell} = \frac{\eta m_{TEOS}}{a^* N_{Za}} \tag{4}$$

Because not all TEOS molecules are converted to SiO_2 particles during the reaction, and some of them are lost during the wash treatment, the yield of TEOS, η, was multiplied by the mass of TEOS, m_{TEOS}. In addition, m_{shell} was calculated by subtracting the mass of the ZnO core from that of the core–shell particles, as shown below:

$$\frac{\eta m_{TEOS}}{a^* N_{Za}} = \frac{4}{3}\pi\left(r_{cs}{}^3 \rho_{SiO_2} - r_c{}^3 \rho_{ZnO}\right) \tag{5}$$

r_{cs} and r_c denote the radii of the core–shell structure and the core particle, respectively. ρ_{SiO_2} and ρ_{ZnO} represent the densities of silica and ZnO, respectively. The silica shell thickness was obtained by subtracting the core radius from the core–shell particle radius. Therefore, the shell thickness r_s was calculated by rearranging eqn (5), as follows:

$$r_s = \left[\frac{3}{4\pi}\left(\frac{\eta m_{TEOS}}{a^* N_{Za}\rho_{SiO_2}} + r_c{}^3 \frac{\rho_{ZnO}}{\rho_{SiO_2}}\right)\right]^{1/3} - r_c \tag{6}$$

A comparison of the shell thickness values obtained based on theoretical calculations and actual measurements from the TEM images is shown in Fig. 4. With the increase in ratio from 0.25 to 1.00, the measured shell thickness was in accordance with the theoretical value. The slight deviation may be caused by the

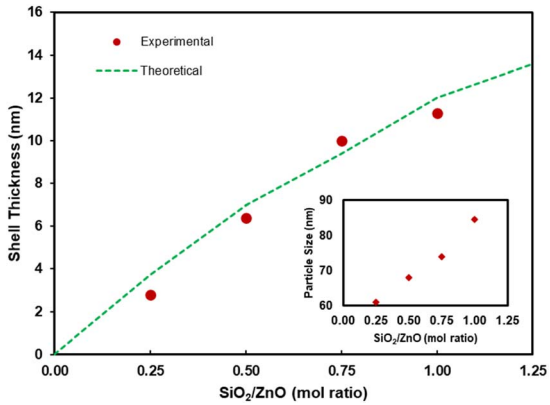

Fig. 4 Average shell thicknesses (inset: core–shell particle diameter) of the core–shell particles formed at various SiO_2/ZnO ratios.

agglomeration of the ZnO core. The experimental results show that the shell thickness tended to increase from 2.8 to 6.9 nm with increasing concentrations of TEOS, as depicted in Fig. 4. Therefore, this mechanism did not involve one ZnO particle covered by silica particles. However, the average size of the ZnO particle showed a narrow distribution. The average core–shell particle size increased from 61.15 to 74.79 nm as the TEOS to ZnO ratio increased from 0.25 to 1.00. The particle size distribution of the SiO_2/ZnO core–shell is shown in the inset of Fig. 4. Furthermore, the ultrasonication process and the addition of higher amounts of SiO_2 particles could reduce agglomeration.

The distribution of ZnO and SiO_2 in the core–shell particles was investigated by elemental mapping of Zn, Si, and O using EDX analysis as shown in Fig. 5. The EDX results provided quantitative confirmation of the elemental composition, ensuring that the desired components were present in the expected proportions. This information is crucial for validating the synthesis process. When the SiO_2/ZnO ratio was 0.25, the ZnO and SiO_2 particles were well-dispersed in the core–shell structure. The EDX analysis confirmed the presence of zinc (Zn), oxygen (O), and silicon (Si). Furthermore, the EDX mappings demonstrated the homogeneity of elemental distribution, reinforcing the uniformity observed in the TEM images. These results further confirm that the ultrasonication treatment not only increases the rate of the reaction but also reduces the agglomeration of the ZnO particles.

To understand the UV attenuation properties, the SiO_2/ZnO particles were tested for photocatalytic activity toward methylene blue (MB) and methyl orange (MO) under sunlight irradiation. Pure ZnO was used in the photocatalytic test for comparison with the core–shell particles. The qualitative results obtained in the MB solution showed that the pure ZnO particles possessed higher photocatalytic activity, as depicted in Fig. 6. After a 30 minutes reaction, the MB solution was completely degraded. In contrast, the core–shell particles in the MB solution displayed reduced photocatalytic activity. After 180 minutes of the photocatalytic test using the core–shell particles, no clear solution was obtained. Almost all samples using core–shell particles showed the same phenomenon. These clearly confirm that the core–shell particles can degrade the MB solution but with lower efficiency.

Further quantitative analysis was conducted by measuring the absorbance of the remaining MB and MO solutions. The results shown in Fig. 7(a) confirm that the adsorption mechanism was dominant when the photocatalytic activity was

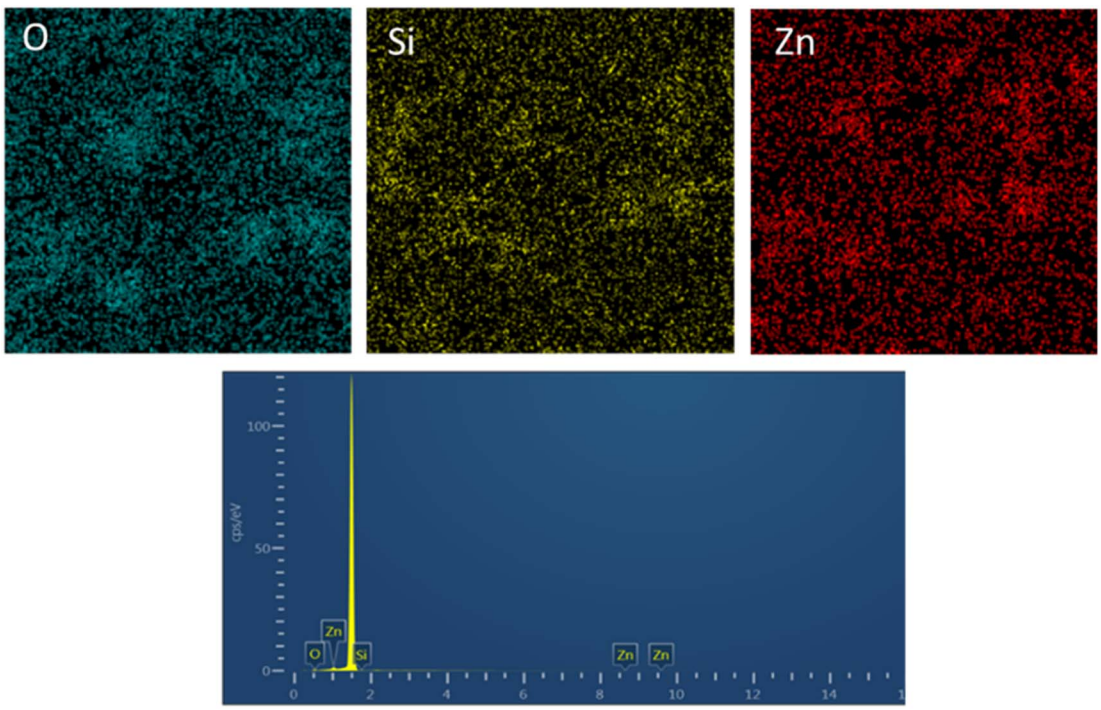

Fig. 5 Elemental mapping of Si, Zn, and O at the SiO_2/ZnO prepared under a ratio of 0.25.

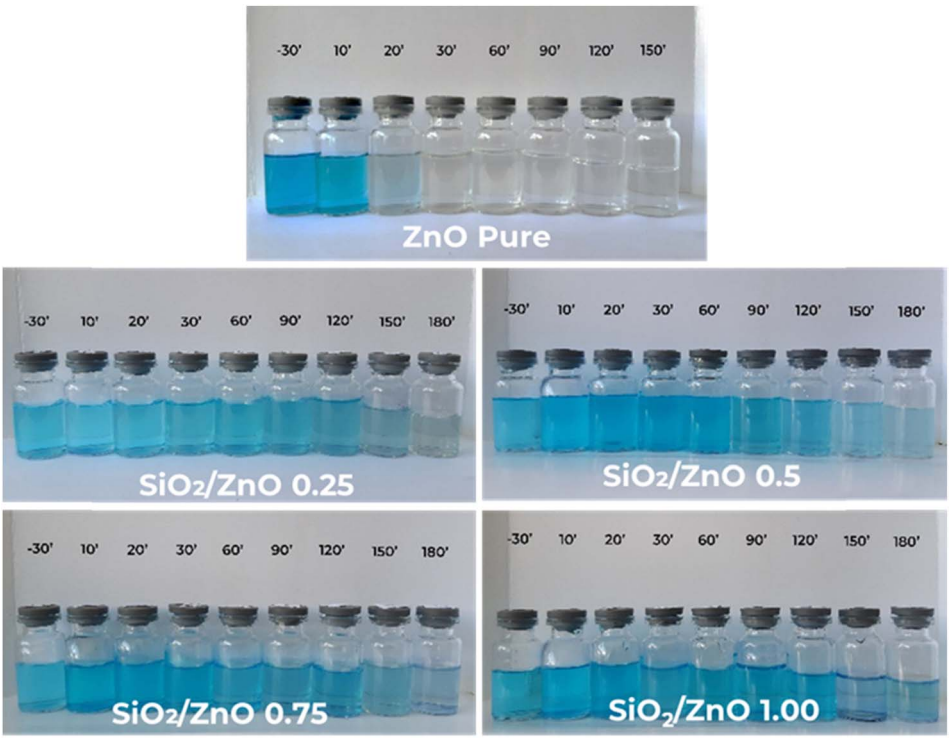

Fig. 6 Qualitative images of the remaining MB solutions after the photocatalytic test using pure ZnO and the core–shell particles.

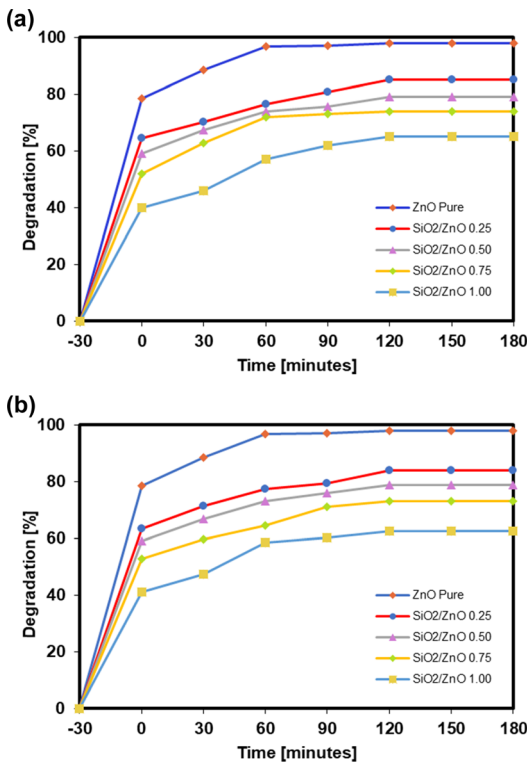

Fig. 7 Photocatalytic activity of pure ZnO and the core–shell particles formed at various SiO_2/ZnO molar ratios in (a) MB solution and (b) MO solution.

conducted in dark conditions for 30 min. The average amount of the MB solution decreased by only 8% in almost all the samples. The pure ZnO particles could degrade 98% of MB within 30 minutes of the photocatalytic reaction. The application of core–shell particles containing different amounts of silica particles also effectively reduced the MB solution but demonstrated lower activity. The 0.25 SiO_2/ZnO ratio sample could degrade the MB solution up to a maximum of 85% after 180 minutes of sunlight irradiation. Moreover, the degradation of MB decreased from 74% to 65% at the same irradiation time when the molar ratio in the core–shell particles changed from 0.5 to 1.00, respectively. This implies that silica coverage can effectively reduce the photocatalytic activity of the ZnO particles. The addition of increasing amounts of silica particles increases the shell thickness, as discussed previously. The silica particles inhibit the interaction of the active site of the ZnO particles with the MB solution. Therefore, the core–shell particles exhibit attenuated photocatalytic degradation of the MB solutions.

The same results were also observed when the core–shell particles were applied to degrade MO solutions. Fig. 7(b) shows that pure ZnO had superior photocatalytic activity, with 98% MO degradation within 30 minutes. The SiO_2/ZnO = 0.25 sample could reduce 83.9% of the MO solution after 180 minutes of irradiation. This is slightly lower compared to the MB solution. MO has a more complicated chemical composition and higher molecular weight, due to which it takes more time to degrade *via* photocatalytic reactions. With an increase in silica molar ratio from 0.50 to 1.00, the degradation of MO decreased from 78.8% to 62.4%. These results clearly indicate

that even when the agglomeration of ZnO particles is reduced by ultrasonication, the presence of silica particles on the outer shell effectively reduces the photocatalytic activity. Reduced photocatalytic activity of the core–shell particles implies limited oxidation–reduction reactions. When the core–shell particles are applied in optical devices, such as lenses and solar cells, or cosmetic applications, such as sunscreen, this reaction is hindered. This is because it promotes the production of active oxygen, which oxidizes other materials, thereby impeding useful optical properties.

Further investigation regarding the inhibition of the photocatalytic activity of the core–shell particles was conducted by measuring their absorbance. Fig. 8(a) shows the absorbance measured in the UVA and UVB wavelength regions from 280–400 nm. The absorbance tended to increase at higher wavelengths from 360 to 400 nm. The highest absorbance was achieved by the core–shell particles prepared with a silica ratio of 1.00. This may happen due to the presence of additional silica particles that absorb more UV light. Moreover, samples with good dispersion showed higher absorption of UV light. This implies that the ultrasonic treatment not only increases particle dispersion but also increases the UV absorption of the particles. Additional investigations on the stability of the core–shell particle dispersion were conducted, and the results are presented in Fig. 8(b). The dispersion was prepared at the concentration of 2 mg mL^{-1}. It was periodically evaluated by measuring the absorbance at 320 and 420 nm over 7 days. The UV-vis measurement results in Fig. 8(b) clearly indicate that the dispersion was stable during the measurement period. The absorbance did not change and showed the average values of 42% and 56% at wavelengths 320 nm and 420 nm, respectively.

To understand the optical properties of the produced core–shell particles, further evaluation was conducted by measuring the photoluminescence (PL) properties. The PL spectra of the produced ZnO particles were evaluated by measuring PL emission. The investigation of the PL properties of the SiO_2/ZnO composite yielded noteworthy findings, shedding light on their optical behaviour and potential applications. Fig. 9 shows the PL spectra of pure ZnO particles when the sample was excited at various UV wavelengths from 230 to 350 nm. The PL spectrum of pure ZnO exhibited distinct emission peaks. The 3D excitation–emission spectra showed that the highest emission peaks corresponding to the excitations wavelengths 230, 260, 290, 320, and 350 nm were located at 466, 524, 584, 644, and 704 nm, respectively, as shown in Fig. 9(a). These contribute to the visible-light emission of blue to red luminescence and possessed the bandgap values of 2.66, 2.36, 2.12, 1.92, and 1.76 corresponding to the excitation–emission spectra. In contrast, Ajiz *et al.*[28] synthesized micro-sized ZnO particles measuring 2.75 μm through a spray-drying method. The ZnO particles possessed only a single PL emission peak at 533 nm corresponding to the green luminescence region. ZnO particles produced in a previous study conducted by Widiyastuti *et al.*[29] also resulted in similar single PL spectra around green bands. The ZnO particles produced in this study showed different PL spectra than those of most reported ZnO particles of the micrometre scale. This result suggests that different particle sizes of ZnO can potentially result in different emission spectra. The particle size can be affected by the synthesis method. In this case, the ultrasonication method produced ZnO particles of nanometre size. It can be concluded that the synthesis method also highly affects the PL spectra. One possible explanation for the differences in the PL spectra is the huge difference in particle size ranging from micrometre to nanometre scale. In the nanometre range, the particle size has a great influence on the PL spectra. In this case, the light was mostly absorbed during particle excitation. The homogenous particle size in nanometre scale showed optimize light absorption. This will lead to the higher intensity in the luminescence measurements. Additionally, the nanometre-sized particles potentially showed improved defect-related PL emission due to oxygen vacancies and zinc interstitials. These results reveal that the particle size has an important role in determining the PL intensity of the ZnO particles. Controlling the size and distribution of the ZnO nanoparticles is crucial for tailoring the optical properties of the composite.

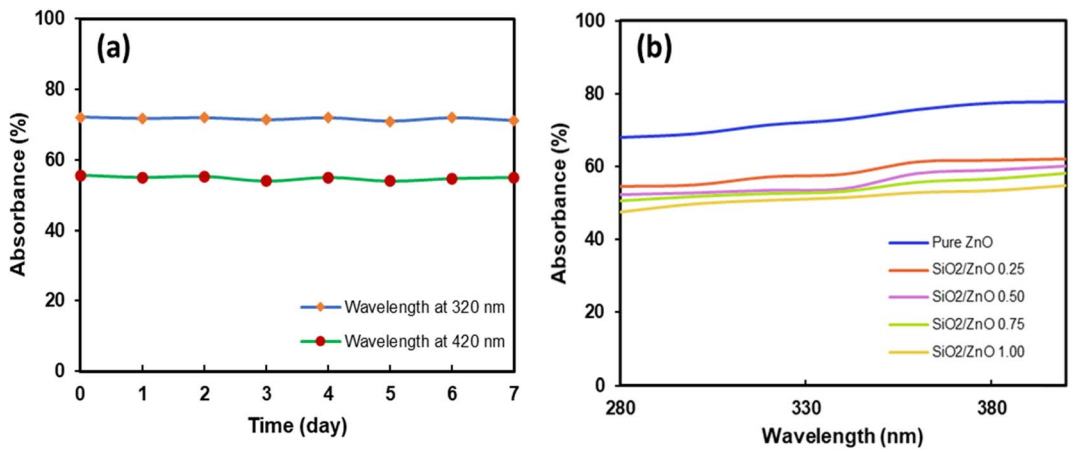

Fig. 8 (a) Stability of the SiO_2/ZnO 0.75 core–shell particle dispersion over time. (b) Optical transmittance spectra of ZnO and core–shell particles containing different ratios of silica.

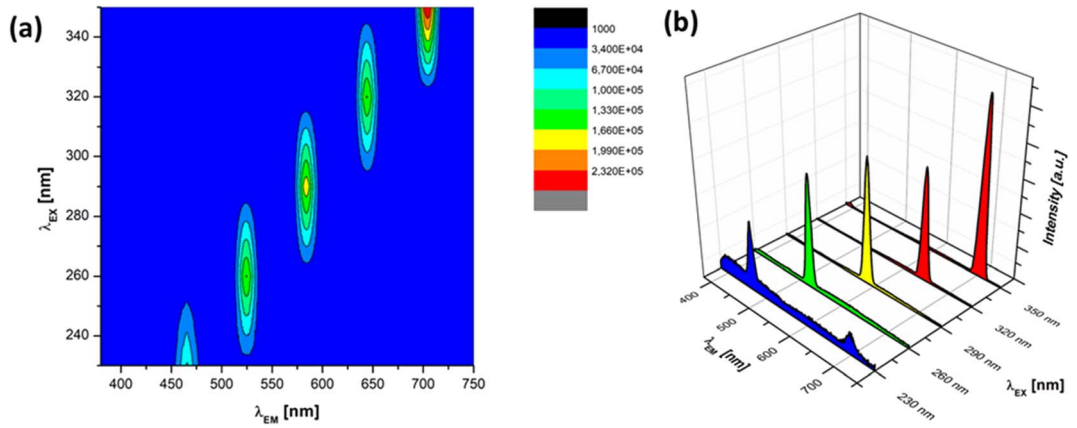

Fig. 9 (a) 3D excitation–emission spectra and (b) single PL emission spectra of the pure ZnO at various UV excitation wavelengths.

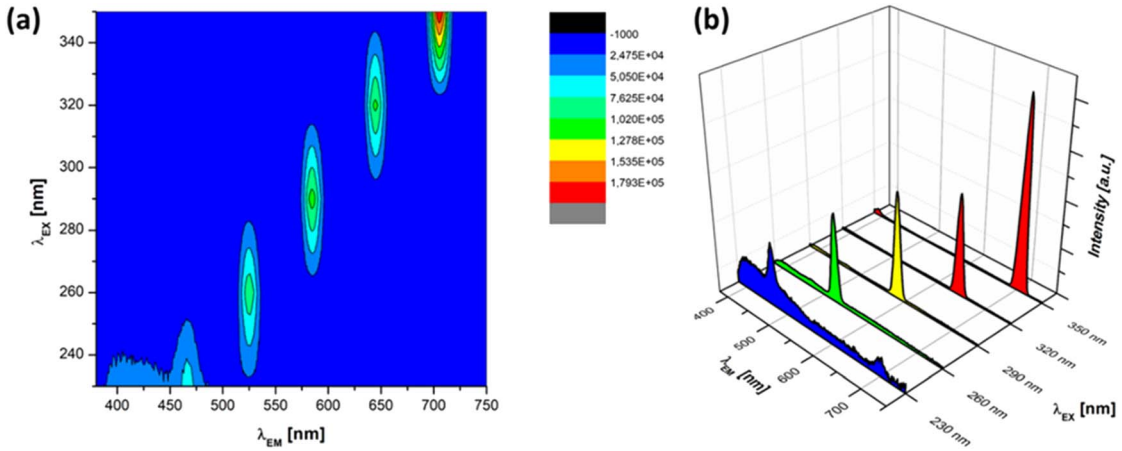

Fig. 10 (a) 3D excitation–emission spectra and (b) single PL emission spectra of the SiO_2/ZnO core–shell particles at various UV excitation wavelengths.

In contrast, after the addition of silica particles, the PL intensity at all excitation wavelengths decreased compared with those of pure ZnO particles, as shown in Fig. 10. The core–shell particles corresponded to the silica ratio of 0.75. The sample was excited at various UV excitation wavelengths from 230 to 350 nm. The 3D excitation–emission spectra showed the highest emission peaks for excitation wavelengths 230, 260, 290, 320, and 350 nm were located at 466, 526, 585, 645, and 705 nm, respectively, as shown in Fig. 10(a). These also contribute to the visible-light emission of blue to red luminescence with a bandgap energy nearly the same as pure ZnO particles. The observed emission peaks in the UV range were consistent with the near-band edge emission of ZnO, suggesting that the composite maintains its characteristic optical properties. The confinement effects induced by the SiO_2 matrix may contribute to shifts in the emission wavelengths and variations in the bandgap energy. However, all the peaks decreased by around 50% compared with pure ZnO. This supports the previous observations from the UV absorption spectra that the presence of silica particles turns out the lower absorption spectra. The presence of silica particles helps increase light scattering, which leads to a reduction in the intensity of PL spectra. This implies that the produced core–shell structure can be attributed to the UV attenuation properties of the produced core–shell particles. The PL results suggest that the SiO_2/ZnO core–shell particle has potential applications in UV attenuation. Further studies can focus on optimizing the core–shell structure to enhance other optical properties, exploring the impact of the synthesis parameters on defect-related emissions, and evaluating material stability over time.

Conclusions

In summary, the synthesis of SiO_2/ZnO core–shell particles using an ultrasound-assisted method proves to be a promising approach, offering nanoparticles with distinctive optical characteristics. This method is effective in producing SiO_2/ZnO composite particles with a well-defined microstructure. The use of ultrasound waves during the synthesis likely plays a crucial role in promoting homogeneous distribution and effective dispersion of the ZnO nanoparticles, along with attachment to the SiO_2 matrix. Therefore, the presence of the silica matrix also

suppresses ZnO agglomeration. This method has the advantage of being relatively simple and energy-efficient. Pure ZnO particles exhibited various excitation–emission behaviours from blue to red luminescence, which does not appear in the micrometre-scale particles. The TEM analysis revealed the uniform distribution of silica in the outer shell, contributing to the well-structured core–shell structure. The outer shell could easily be tuned by changing the silica ratio from 0.25 to 1.00. The shell thickness was uniform and varied from 2.8 to 11.3 nm as the silica ratio was changed. The optical parameters, such as optical transmittance and PL measurements uncovered key aspects of the core–shell behaviour. Increasing the silica ratio effectively reduced ZnO agglomeration and UV scattering. The observed high UV absorbance and lower PL intensity indicate the efficient optical properties of the SiO_2/ZnO core–shell structure, highlighting its potential in UV attenuation applications. The integration of ultrasound as a synthesis tool has proven to be effective in achieving a well-defined structure, and the observed optical properties suggest its potential for applications in various technological domains.

Author contributions

Lailatul Qomariyah: conceptualization, writing – review & editing. Tomoyuki Hirano: visualization, writing – review & editing. Nicky Rahmana Putra: writing – review & editing. Suprapto Suprapto: writing – review & editing. Hendrix Abdul Ajiz: investigation, writing – review & editing. Mar'atul Fauziyah, writing – review & editing.

Conflicts of interest

The authors declare that they have no conflict of interest such as financial or personal relationship that influence the work reported in this paper.

Acknowledgements

This work is financially supported in part by a grant from Directorate of Research and Public Service, Institut Teknologi Sepuluh Nopember (L. Q.) under contract number 0041/01.PKS/PPK-HETI/ITS/2023. The author also greatly acknowledges to the financial support provided by Kurita Water and Environment Foundation (L. Q.) under contract ID 23Pid158. We also extend our gratitude to Anisa Tiara Damayanti and Ramadhani Yusdhaliyanti Anwar for the assistance of the experiment.

References

1 J. Y. Huang, G. T. Fei, S. H. Xu and B. Wang, *Composites, Part B*, 2023, **251**, 110486.
2 Z. Cao, Z. Zhang, F. Wang and G. Wang, *Colloids Surf., A*, 2009, **340**, 161–167.
3 T. Iwasaki, M. Satoh and S. Ichio, *J. Mater. Process. Technol.*, 2003, **142**, 131–138.
4 C.-H. Xue, W. Yin, P. Zhang, J. Zhang, P.-T. Ji and S.-T. Jia, *Colloids Surf., A*, 2013, **427**, 7–12.
5 Z. Sun, T. Liao, Y. Dou, S. M. Hwang, M.-S. Park, L. Jiang, J. H. Kim and S. X. Dou, *Nat. Commun.*, 2014, **5**, 3813.
6 K. Al-Attafi, A. Al-Keisy, M. A. Alsherbiny and J. H. Kim, *Sci. Technol. Adv. Mater.*, 2023, **24**, 2277678.
7 N. Hagura, T. Takeuchi, S. Takayama, F. Iskandar and K. Okuyama, *J. Lumin.*, 2011, **131**, 138–146.
8 J. H. Hong, Y. F. Wang, G. He and J. X. Wang, *J. Non-Cryst. Solids*, 2010, **356**, 2778–2780.
9 L. Shastri, M. S. Qureshi and M. M. Malik, *J. Phys. Chem. Solids*, 2013, **74**, 595–598.
10 A. Kadir, L. Qomariyah, T. Ogi, H. Atmajaya, N. R. Putra, S. D. A. M. Sunarno, M. Tejamaya and D. R. Zuchrillah, *J. Sol-Gel Sci. Technol.*, 2023, **107**, 711–724.
11 R. Georgekutty, M. K. Seery and S. C. Pillai, *J. Phys. Chem. C*, 2008, **112**, 13563–13570.
12 X. Chen, Z. Wu, D. Liu and Z. Gao, *Nanoscale Res. Lett.*, 2017, **12**, 1–10.
13 L.-Y. Yang, S.-Y. Dong, J.-H. Sun, J.-L. Feng, Q.-H. Wu and S.-P. Sun, *J. Hazard. Mater.*, 2010, **179**, 438–443.
14 L. Qomariyah, W. Widiyastuti, K. Kusdianto, T. Nurtono, D. Anggoro and S. Winardi, *Chem. Pap.*, 2020, **74**, 4115–4123.
15 N. Hagura, T. Ogi, T. Shirahama, F. Iskandar and K. Okuyama, *J. Lumin.*, 2011, **131**, 921–925.
16 W. J. Guedens, M. Reynders, H. Van den Rul, K. Elen, A. Hardy and M. K. Van Bael, *J. Chem. Educ.*, 2014, **91**, 259–263.
17 K.-B. Kim, Y. W. Kim, S. K. Lim, T. H. Roh, D. Y. Bang, S. M. Choi, D. S. Lim, Y. J. Kim, S.-H. Baek and M.-K. Kim, *J. Toxicol. Environ. Health, Part B*, 2017, **20**, 155–182.
18 E. Spisni, S. Seo, S. H. Joo and C. Su, *Int. J. Environ. Sci. Technol.*, 2016, **13**, 2485–2494.
19 S. Baek, S. H. Joo, N. Kumar and M. Toborek, *J. Environ. Chem. Eng.*, 2017, **5**, 3024–3032.
20 K. Kusdianto, W. Widiyastuti, M. Shimada, L. Qomariyah and S. Winardi, *IOP Conf. Ser.: Mater. Sci. Eng.*, 2020, **778**(1), 1–10.
21 L. Qomariyah, M. Aisah, N. Cahyando, W. Widiyastuti and S. Winardi, *AIP Conf. Proc.*, 2017, **1840**(1), 080009.
22 S. S. Alias, A. B. Ismail and A. A. Mohamad, *J. Alloys Compd.*, 2010, **499**, 231–237.
23 A. M. Abdelmonem, B. Pelaz, K. Kantner, N. C. Bigall, P. Del Pino and W. J. Parak, *J. Inorg. Biochem.*, 2015, **153**, 334–338.
24 S. U. Ilyas, R. Pendyala and N. Marneni, *Mater. Res. Innovations*, 2014, **18**, S6–S179.
25 M. M. Hossain, M. A. Islam, H. Shima, M. Hasan, M. Hilal and M. Lee, *RSC Adv.*, 2018, **8**, 16927–16936.
26 K.-C. Choi, E.-J. Lee, Y.-K. Baek, M.-J. Kim, Y.-D. Kim, P.-W. Shin and Y.-K. Kim, *RSC Adv.*, 2014, **4**, 7160–7166.
27 S. K. Mishra, U. K. Tripathi, R. R. Awasthi, R. K. Shukla, I. Kumar, R. M. Naik and D. P. Mishra, *Mater. Today: Proc.*, 2021, **46**, 2229–2234.
28 H. A. Ajiz, K. Santoso, J. A. Purnama, W. Widiyastuti, T. Nurtono and H. Setyawan, *Adv. Powder Technol.*, 2023, **34**, 104181.
29 W. Widiyastuti, I. Maula, T. Nurtono, F. Taufany, S. Machmudah, S. Winardi and C. Panatarani, *Chem. Eng. J.*, 2014, **254**, 252–258.

30 H. J. Zhang, H. M. Xiong, Q. G. Ren, Y. Y. Xia and J. L. Kong, *J. Mater. Chem.*, 2012, **22**, 13159–13165.
31 A. E. Raevskaya, Y. V Panasiuk, O. L. Stroyuk, S. Y. Kuchmiy, V. M. Dzhagan, A. G. Milekhin, N. A. Yeryukov, L. A. Sveshnikova, E. E. Rodyakina and V. F. Plyusnin, *RSC Adv.*, 2014, **4**, 63393–63401.
32 F. H. Saboor, A. A. Khodadadi, Y. Mortazavi and M. Asgari, *Sens. Actuators, B*, 2017, **238**, 1070–1083.
33 T. Tani, L. Mädler and S. E. Pratsinis, *J. Mater. Sci.*, 2002, **37**, 4627–4632.
34 R. Ayouchi, F. Martin, D. Leinen and J. R. Ramos-Barrado, *J. Cryst. Growth*, 2003, **247**, 497–504.
35 B.-A. Kang, K.-S. Hwang and J.-H. Jeong, *J. Sol-Gel Sci. Technol.*, 2007, **43**, 145–149.
36 R. Ullah and M. Tuzen, *Surf. Interfaces*, 2023, **39**, 102918.
37 S. Khanna, M. Kiruthika, S. Chidambaram and M. Rathinam, *Mater. Sci. Eng. B*, 2023, **293**, 116484.
38 L. F. M. Ismail, M. M. Emara, M. M. El-Moselhy, N. A. Maziad and O. K. Hussein, *Spectrochim. Acta, Part A*, 2014, **131**, 158–168.
39 B. Arik and O. D. Karaman Atmaca, *Cellulose*, 2020, **27**, 8385–8403.
40 S. Qiu, H. Zhou, Z. Shen, L. Hao, H. Chen and X. Zhou, *RSC Adv.*, 2020, **10**, 2767–2785.
41 S. Kumar, R. Seth, S. Panwar, K. K. Goyal, V. Kumar and R. K. Choubey, *J. Electron. Mater.*, 2021, **50**, 3462–3470.
42 G.-C. Lee, L.-M. Lyu, K.-Y. Hsiao, Y.-S. Huang, T.-P. Perng, M.-Y. Lu and L.-J. Chen, *Nano Energy*, 2022, **93**, 106867.
43 L. Qomariyah, A. F. Arif, W. Widiyastuti, S. Winardi, S. Taniguchi and T. Ogi, *RSC Adv.*, 2018, **8**, 26277–26282.
44 A. F. Arif, Y. Kobayashi, R. Balgis, T. Ogi, H. Iwasaki and K. Okuyama, *Carbon*, 2016, **107**, 11–19.
45 D. B. Kaustar, M. F. Rois, N. Faizah, W. Widiyastuti, T. Nurtono, H. Setyawan and P. Poly, *Chem. Eng.*, 2023, **67**, 161–171.